An electrochemical model of lithium plating and stripping in lithium-ion batteries

Simon Hein,[*,†,‡] Timo Danner,[†,‡] and Arnulf Latz[†,‡,¶]

†*German Aerospace Center (DLR), Institute of Engineering Thermodynamics,Pfaffenwaldring 38-40,70569 Stuttgart, Germany*

‡*Helmholtz Institute for Electrochemical Energy Storage (HIU), Helmholtzstraße 11, 89081 Ulm, Germany*

¶*Ulm University (UUlm), Institute of Electrochemistry, Albert-Einstein-Allee 47, 89081 Ulm, Germany*

E-mail: simon.hein@dlr.de

Abstract

The deposition of a metallic lithium phase on the surface of graphite anodes in lithium-ion batteries is a major degradation process and causes inherent safety risks. Despite its importance for battery applications the detection of this so-called lithium plating process during battery charge is very challenging. Therefore, a mechanistic understanding of the Li plating mechanism and the identification of characteristic features in the charge curve of the battery are extremely important. We present an electrochemical model, which enables the description of the deposition and dissolution of a metallic lithium phase in 3D micro-structure resolved simulations of lithium-ion batteries. The features of this model are demonstrated by simulating the overcharge of a graphite electrode in half-cell configuration. Simulation results show the typical features of the 'stripping-plateau' which is often observed during discharge after Li plating occurred. Moreover, a similar feature is observed at the onset of Li plating which can serve as

an indicator for lithium plating in lithium-ion batteries during charging e.g. of electric vehicles. Finally, we investigate the impact of an inhomogeneous solid-electrolyte-interphase on the distribution of plated lithium which highlights the effect of local structural heterogeneities on degradation phenomena.

Keywords

Lithium-Ion Battery, Model of lithium plating and stripping, Microstructure resolved simulation, Inhomogeneous SEI, Graphite

1 Introduction

The deposition of metallic lithium on the surface of graphite electrodes is one of the major degradation mechanisms in lithium-ion batteries (LIB). The term *lithium plating* is often used in the lithium-ion battery community to describe this process.[1] Lithium plating usually occurs during operation of the battery at low temperatures or high charging currents. Detection of this phenomenon is not straight forward and often only indirect proof is given through the aging behavior,[2,3] the discharge cell voltage[4] or post-mortem-analysis.[5] A direct detection of lithium plating requires complex experimental setups, i.e. electrochemical cells with optical windows,[6–8] or expensive instruments, i.e. nuclear magnetic resonance instruments.[9–12] These approaches provide a mechanistic understanding, however, are not feasible in practical applications. Electrochemical models provide another route for detection and identification of hardly accessible processes, e.g. lithium plating. Designated model experiments can be used to validate models, which include a description of lithium plating and stripping. These electrochemical models can then help to detect lithium plating during operation of a battery cell in a more realistic battery environment. The main challenge of the modeling of lithium plating in lithium-ion batteries is the description of the plating reaction and the morphology of the plated lithium. The competition between the intercalation reac-

tion and the plating reaction, as well as the influence of the electrode microstructure on the localization of lithium plating introduce additional complexities.

The electrodeposition of metals is a well studied field in electrochemistry. The process of lithium plating in LIB differs from the process of metal plating on metallic substrates. A feature of LIBs is the intercalation electrode, where the lithium is stored in a host material, e.g. graphite. Therefore, the deposition of metallic lithium onto the electrodes competes with the intercalation of lithium into the active material. In contrast, electrodeposition theories commonly neglect the presence of competing reactions.[13–15]

In lithium-ion battery research several different models exist, which try to describe the deposition of metallic lithium on the surface of graphite particles. While most work focuses on the possible structural growth mechanisms of lithium surface films and dendrites (diffusion limited, field gradients),[13,16–19] Arora *et al.*[20] were one of the first to use an electrocemical model to investigate the effect of lithium plating on the performance of a LIB. This model is based on the volume averaged porous electrode theory[21] combined with the description of the plated lithium as an additional reaction.[20] Moreover, a lumped model is used to describe the effect of the metallic lithium phase and the solid-electrolyte-interphase on the intercalation of lithium ions in graphite. Several publications use the model of Arora as a basis to investigate the impact of temperature,[22] a lateral misalignment between anode and cathode,[23] or the influence of prolonged cycling.[24] Later on the model was extended to allow for lithium stripping.[25,26] These models have in common, that inhomogeneities on the particle level can not be resolved.[27] Also, the surface of the electrode available for intercalation is not influenced by the metallic lithium. Thus, even a significant amount of plated lithium will not suppress the intercalation into the active material. Recently, Baker formulated a description, which also includes the coverage of the particle surface, but still restricted to a volume average description and single particle simulations.[28] The authors are not aware of any modeling studies investigating the deposition of Li on metal substrate or even graphite in 3D spatially resolved simulations.

Aim of this work is the integration of a detailed model describing the formation and dissolution of a metallic lithium phase on the surface of the graphite particles in the microstructure of a lithium-ion battery anode. The model is embedded in a thermodynamically consistent modeling framework[29,30] implemented in the Battery and Electrochemistry Simulation Tool BEST.[31] Thus, resulting in a extended simulation software, which allows the simulation of lithium plating under various conditions in realistic anode micro-structures. The constitutive equations of the transport model are presented in Table 1. These equations correspond to the isothermal case of the transport model as derived in Ref. 29 and 30. In contrast to other

Table 1: The constitutive equations of the isothermal Li-ion battery model used in this work. Details of the derivation can be found in the references.[29,30] The definition of the different symbols and parameters can be found in the list of symbols at the end of the manuscript.

Phase	Material balance	Charge balance
Electrolyte	$\frac{\partial c_{\mathrm{El}}}{\partial t} = -\vec{\nabla} \cdot \vec{N}_{El}$	$0 = -\vec{\nabla} \cdot \vec{j}_{El}$
Active material	$\frac{\partial c_{\mathrm{So}}}{\partial t} = -\vec{\nabla} \cdot \vec{N}_{So}$	$0 = -\vec{\nabla} \cdot \vec{j}_{So}$
Phase	Lithium flux	Charge flux
Electrolyte	$\vec{N}_{\mathrm{El}} = -D_{\mathrm{El}} \vec{\nabla} c_{\mathrm{El}} + \frac{t_{\pm}}{F} \vec{j}_{\mathrm{El}}$	$\vec{j}_{\mathrm{El}} = -\kappa_{\mathrm{El}} \vec{\nabla} \varphi_{\mathrm{El}} + \kappa_{\mathrm{El}} \frac{1-t_{\pm}}{F} \left(\frac{\partial \mu_{\mathrm{El}}}{\partial c_{\mathrm{El}}} \right) \vec{\nabla} c_{\mathrm{El}}$
Active material	$\vec{N}_{\mathrm{So}} = -D_{\mathrm{So}} \vec{\nabla} c_{\mathrm{So}}$	$\vec{j}_{\mathrm{So}} = -\sigma_{\mathrm{So}} \vec{\nabla} \Phi_{\mathrm{So}}$

publications[20] in the literature, the methodology presented in this work allows simulating the transition from intercalation to metallic deposition of lithium onto the graphite surface during charging of the battery. Moreover, the model successfully reproduces the well-known stripping plateau during discharge of a lithium-ion battery, where lithium plating was induced on purpose in the subsequent charge process.[11] Additionally, a feature in the half-cell voltage during battery charge could be identified at the onset of lithium plating which might serve as a characteristic indicator for battery diagnostics. Finally, we shortly touch on the effect of an inhomogeneous solid-electrolyte-interphase (SEI). This serves as a starting point in our continous effort to study limiting processes for anode performance and life time.[32,33,34]

2 Model derivation

The electrochemical model of the graphite-electrolyte-interface describes intercalation of lithium ions in and the growth of a lithium metal film on the surface of the graphite particles in Lithium-ion battery anodes. A schematic representation of the different reactions and processes which are taken into account in this approach are shown in Figure 1.

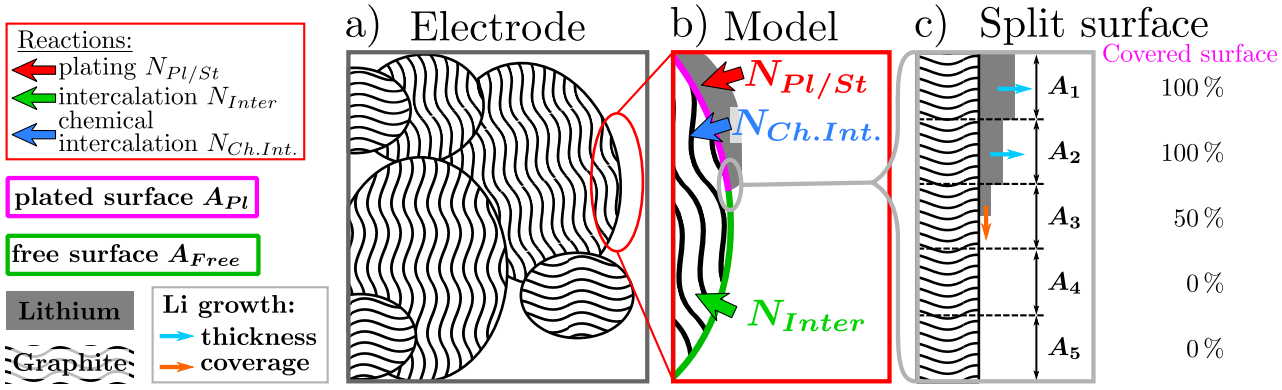

Figure 1: a) Sketch of a graphite electrode consisting of several particles (ellipses with wavy pattern). b) A magnification of the graphite surface with metallic lithium (grey) present. The dissolved lithium in the electrolyte, the plated lithium and the intercalated lithium can react along the three shown paths (arrows). The lithium plating $N_{\mathrm{Pl/St}}$ and the chemical intercalation $N_{\mathrm{Ch.Int.}}$ occur at the covered surface A_{Pl} (purple), while the intercalation N_{Inter} takes place through the interface between graphite and electrolyte A_{Free} (dark green). c) The subdivision of the graphite electrode for the electrochemical simulation is sketched. The plated lithium is tracked on each element, thus allowing for a partial coverage of graphite particles.

Three reactions are relevant: (I) the intercalation reaction between electrolyte and graphite (N_{Inter}), (II) the metallic lithium deposition and stripping ($N_{\mathrm{Pl/St}}$), and (III) a charge-neutral insertion of plated lithium atoms in the supporting graphite host structure ($N_{\mathrm{Ch.Int.}}$). The different processes cannot be studied individually because they are connected through the surface concentration of lithium on the graphite particles. Without the presence of a plated lithium phase (pristine surface), lithium ions intercalate from the electrolyte into the graphite host structure in a one-electron charge transfer reaction

$$\mathrm{Li}^{+}_{\mathrm{Elyte}} + \mathrm{e}^{-} \rightleftharpoons \mathrm{Li}^{0}_{\mathrm{intercalated}} \,. \tag{1}$$

During plating the lithium ions are reduced on the graphite surface and get deposited from the electrolyte forming a neutral lithium atom

$$\mathrm{Li}^{+}_{\mathrm{Elyte}} + \mathrm{e}^{-} \rightleftharpoons \mathrm{Li}^{0}_{\mathrm{plated}} \,. \tag{2}$$

Prolonged deposition results in a growing lithium phase, which eventually covers the whole surface and suppresses the intercalation reaction (N_{Inter}). The metallic lithium on the surface is not thermodynamically stable. It can either re-dissolve in the electrolyte, react with the electrolyte to form solid-electrolyte-interphase, or intercalate via a charge neutral transfer reaction (chemical intercalation) into the supporting graphite

$$\mathrm{Li}^{0}_{\mathrm{plated}} \rightleftharpoons \mathrm{Li}^{0}_{\mathrm{intercalated}} \,. \tag{3}$$

For the description of the reactions in Eq. 1 - Eq. 3 we use a generalized formulation of Butler-Volmer kinetics[35,36]

$$N_r = N_r^0 \cdot \left(\exp\left[\frac{\alpha_r \Delta G_r}{R\,T} \right] - \exp\left[-\frac{(1-\alpha_r)\Delta G_r}{R\,T} \right] \right) \,, \tag{4}$$

where N_r is the lithium flux due to reaction r, ΔG_r the Gibbs free energy of the reaction r, N_r^0 the pre-exponential factor, R the ideal gas constant, T the temperature and α_r the symmetry factor of the transition state. The definition of symbols, subscript and superscript

within this manuscript can be found in Section (5). The reaction is driven by the Gibbs free energy of reaction

$$\Delta G_r = \sum_s \nu_{r,s} \tilde{\mu}_{\mathrm{s}}^{\mathrm{p}} \ , \tag{5}$$

where $\tilde{\mu}_{\mathrm{s}}^{\mathrm{p}}$ is the electrochemical potential of species s in phase p with respect to an arbitrary reference and $\nu_{r,s}$ is the stoichiometric coefficient of species s in reaction r. The electrochemical potential is given through the chemical potential $\mu_{\mathrm{s}}^{\mathrm{p}}$ and the electrical potential Φ^{p} [37]

$$\tilde{\mu}_{\mathrm{s}}^{\mathrm{p}} = \mu_{\mathrm{s}}^{\mathrm{p}} + z_{\mathrm{s}} \cdot F \cdot \Phi^{\mathrm{p}} \ , \tag{6}$$

with z_{s} the charge of species s. The chemical potential can be expressed as a function of the activity a_s^p

$$\mu_{\mathrm{s}}^{\mathrm{p}} = \mu_{\mathrm{s}},^{\mathrm{p},\Theta} + R \cdot T \cdot \log\left(a_{\mathrm{s}}^{\mathrm{p}}\right) \ , \tag{7}$$

where $\mu_{\mathrm{s}},^{\mathrm{p},\Theta}$ is the chemical potential of the reference state Θ.[38] The activity of metals is one per definition. The plating reaction (Eq. 2) and the chemical intercalation (Eq. 3) involve plated lithium. This metallic lithium phase can dissolve completely during stripping. In order to take into account, that the chemical potential of the dissolving/forming metallic lithium phase will deviate from its bulk reference state by e.g. contributions of the surface energy, we use an extended phenomenological expression for the activity of the metallic Li phase

$$\mu_{\mathrm{Li}^0}^{\mathrm{Pl}} = \mu_{\mathrm{Li}^0}^{\Theta} + R \cdot T \cdot \ln\left(\frac{n_{\mathrm{Pl}}^4}{n_{\mathrm{Pl},0}^4 + n_{\mathrm{Pl}}^4}\right) \ . \tag{8}$$

Note, that one obtains the expected bulk activity of one as soon as the amount of plated lithium n_{PL} exceeds a threshold value $n_{PL,0}$. More detailed models for the activity of Li can be included in the expressions, which is part of ongoing research. The common choice of a reference in the Li-ion battery community is metallic Lithium and typically measurements to study the thermodynamics of intercalation materials, that is the open-circuit potential U_0, are performed against a Li metal electrode. The open-circuit potential of the intercalation material can then be expressed by

$$U_0 = \frac{\mu_{\mathrm{Li}}^{\mathrm{Ref}} - \mu_{Li}^{So}}{F} \ , \tag{9}$$

where $\mu_{\mathrm{Li}}^{\mathrm{Ref}}$ is the chemical potential of the reference state. The pre-exponential factor N_r^0 in Eq. 4 is given by a product of the activities[35,36]

$$N_r^0 = K_r^{00} \cdot \frac{\left(c_{\mathrm{Li}}^{So}\right)^{\alpha_c}\left(c_{\mathrm{Li}^+}^{El}\right)^{\alpha_a}}{\left(c_{\mathrm{Li}}^{So,0}\right)^{\alpha_c}\left(c_{\mathrm{Li}^+}^{El,0}\right)^{\alpha_a}} \ , \tag{10}$$

where K_r^{00} is the equilibrium constant of reaction r, $c_{\mathrm{r}}^{p,0}$ is the concentration of species r in the reference state of phase p, α_a is the anodic transfer number and α_c the cathodic transfer number (with $\alpha_a + \alpha_c = 1$). The constant factors can be condensed into the pre-exponential factor

$$N_r^0 = N_r^{00}\left(c_{\mathrm{Li}}^{So}\right)^{\alpha_c}\left(c_{\mathrm{Li}^+}^{El}\right)^{\alpha_a} \ , \tag{11}$$

where rate constant N_r^{00} follows as

$$N_r^{00} = \frac{K_r^{00}}{\left(c_{\mathrm{Li}}^{So,0}\right)^{\alpha_c}\left(c_{\mathrm{Li}^+}^{El,0}\right)^{\alpha_a}} \ . \tag{12}$$

(I) For the *intercalation* reaction (Eq. 1, $r = \mathrm{Inter}$) the free energy of the reaction

$$\Delta G_{\mathrm{Inter}} = \tilde{\mu}_{\mathrm{Li}^0}^{\mathrm{So}} - \tilde{\mu}_{\mathrm{Li}^+}^{\mathrm{El}} - \tilde{\mu}_{\mathrm{e}^-}^{\mathrm{So}} \tag{13}$$

can be rewritten using the definitions of the electrochemical potential (Eq. 6) and open-circuit potential (Eq. 9) according to

$$\Delta G_{\mathrm{Inter}} = F \cdot \Phi^{\mathrm{So}} - F \cdot \Phi^{El} - \left(\mu_{\mathrm{Li}^+}^{\mathrm{El}} - \mu_{\mathrm{Li}}^{\mathrm{Ref}}\right) - F \cdot U_0 \ . \tag{14}$$

The chemical potential of the electrolyte $\mu_{\mathrm{Li}^+}^{\mathrm{El}}$ is different from the reference state $\mu_{\mathrm{Li}}^{\mathrm{Ref}}$. Hence, the difference $\mu_{\mathrm{Li}^+}^{\mathrm{El}} - \mu_{\mathrm{Li}}^{\mathrm{Ref}}$ does not vanish from Eq. 14. The electrochemical potential of the electrolyte $\varphi_{\mathrm{Li}^+}^{\mathrm{El}}$ relative to the lithium reference is introduced to

$$\varphi_{\mathrm{Li}^+}^{\mathrm{El}} = \Phi^{El} + \frac{\mu_{\mathrm{Li}^+}^{\mathrm{El}} - \mu_{\mathrm{Li}}^{\mathrm{Ref}}}{F} \ . \tag{15}$$

The free energy of the *intercalation* reaction (Eq. 14) hence follows as

$$\Delta G_{\mathrm{Inter}} = F \cdot \left(\Phi^{\mathrm{So}} - \varphi_{\mathrm{Li}^+}^{\mathrm{El}} - U_0\right) \ . \tag{16}$$

The common definition of the overpotential η_{inter} is given by

$$\eta_{\mathrm{Inter}} = \Delta G_{\mathrm{Inter}}/F = \Phi^{\mathrm{So}} - \varphi^{\mathrm{El}}_{\mathrm{Li^+}} - U_0;. \tag{17}$$

Following the systematic derivation of the pre-exponential factor $N^0_{\mathrm{Inter}} = N^{00}_{\mathrm{Inter}} \cdot \sqrt{c_{\mathrm{El}} \cdot c_{\mathrm{So}}}$ and assuming a symmetry factor of $\alpha^{\mathrm{a}}_{\mathrm{Inter}} = \alpha^{\mathrm{c}}_{\mathrm{Inter}} = 0.5$ the kinetic expression for the intercalation expression follows as

$$N_{\mathrm{Inter}} = N^{00}_{\mathrm{Inter}} \cdot \sqrt{c_{\mathrm{El}} \cdot c_{\mathrm{So}}} \cdot \left(\exp\left[\frac{F\ \eta_{\mathrm{Inter}}}{2\ R\ T} \right] - \exp\left[-\frac{F \eta_{\mathrm{Inter}}}{2\ R\ T} \right] \right)\ . \tag{18}$$

The resulting equation[35] is similar to the Butler-Volmer-expression, which is commonly used in the field of lithium-ion batteries.[36,39,40]

(II) In the same manner a kinetic expression for the *plating and stripping* of lithium (Eq. 2, $r = \mathrm{Pl/St}$) can be derived. The free energy of the reaction follows as

$$\Delta G_{\mathrm{Pl/St}} = \tilde{\mu}^{\mathrm{Pl}}_{\mathrm{Li^0}} - \tilde{\mu}^{\mathrm{El}}_{\mathrm{Li^+}} - \tilde{\mu}^{\mathrm{Pl}}_{\mathrm{e^-}}\ . \tag{19}$$

The resulting overpotential taking into account the chemical potential of plated lithium of the plating/stripping reaction follows as

$$\eta_{\mathrm{Pl/St}} = \Phi^{\mathrm{So}} - \varphi^{\mathrm{El}}_{\mathrm{Li^+}} + \frac{R \cdot T}{F} \cdot \ln\left(\frac{n^4_{\mathrm{Pl}}}{n^4_{\mathrm{Pl},0} + n^4_{\mathrm{Pl}}} \right)\ . \tag{20}$$

Note, that the last term of the equation is a result of the phenomenological activity expression presented in Eq. 8. In the derivation we assume that ohmic losses in the Li metal are negligible and $\Phi^{\mathrm{Pl/St}} = \Phi^{\mathrm{So}}$. The symmetry factor of the reaction was measured to

$\alpha^{\mathrm{a}}_{\mathrm{Pl/St}} \approx 0.3$.[41] The pre-exponential factor is given by $N^{0}_{\mathrm{Pl/St}} = N^{00}_{\mathrm{Pl/St}} \cdot (c_{\mathrm{El}})^{\alpha^{\mathrm{a}}_{\mathrm{Pl/St}}}$. The kinetic expression of the plating/stripping reaction finally follows as

$$N_{\mathrm{Pl/St}} = N^{00}_{\mathrm{Pl/St}} \cdot (c_{\mathrm{El}})^{0.3} \cdot \left(\exp\left[\frac{0.3\ F\ \eta_{\mathrm{Pl/St}}}{R\ T} \right] - \exp\left[-\frac{0.7\ F\ \eta_{\mathrm{Pl/St}}}{R\ T} \right] \right) . \tag{21}$$

(III) The plated lithium on the surface of the graphite is not in an thermodynamically stable configuration. The free energy for the *chemical intercalation* (Eq. 3, r = Ch.Int.) is given by

$$\Delta G_{\mathrm{Ch.Int.}} = \tilde{\mu}^{\mathrm{Pl}}_{\mathrm{Li^0}} - \tilde{\mu}^{\mathrm{So}}_{\mathrm{Li^0}} . \tag{22}$$

Following the definitions of chemical potentials for Li in the graphite host structure (Eq. 9) and the plated lithium phase (Eq. 8) the overpotential of the chemical intercalation is given by

$$\eta_{\mathrm{Ch.Int.}} = -U^{so}_{0}(c^{so}_{Li}) - \frac{R \cdot T}{F} \cdot \ln\left(\frac{n^{4}_{\mathrm{Pl}}}{n^{4}_{\mathrm{Pl},0} + n^{4}_{\mathrm{Pl}}} \right) . \tag{23}$$

Due to a lack of experimental data the symmetry factor is assumed to $\alpha_{\mathrm{Ch.Int.}} \approx 0.5$ and the pre-exponential factor follows from the derivation to $N^{0}_{\mathrm{Ch.Int.}} = N^{00}_{\mathrm{Ch.Int.}} \cdot \sqrt{c_{\mathrm{So}}}$. The final kinetic expression for the chemical intercalation is given by

$$N_{\mathrm{Ch.Int.}} = N^{00}_{\mathrm{Ch.Int.}} \cdot \sqrt{c_{\mathrm{So}}} \cdot \left(\exp\left[\frac{F\ \eta_{\mathrm{Ch.Int.}}}{2\ R\ T} \right] - \exp\left[-\frac{F\ \eta_{\mathrm{Ch.Int.}}}{2\ R\ T} \right] \right) . \tag{24}$$

Generally, the current flux through the interface is given with $j_r = N_r \cdot F$.[42] Note, that in the case of chemical intercalation the charge transfer occurs during the plating/stripping reaction and the subsequent chemical intercalation step does not contribute to the Farradaic current ($j_{\text{Ch.Int.}} = 0$).

Experimental investigations of lithium deposition on lithium substrate showed, that after an initial thickness growth different morphologies, which are described as "bushy" or "dense" structures, evolve.[6,12] The local electrochemical conditions which lead to the development of one morphology or the other are not fully understood. Within this porous lithium phase depletion of lithium ions in the electrolyte close to the substrate is reported.[16] This transport limitation together with tip effects reduces the electrochemical active region to only the fraction of the porous surface close to the electrolyte interface.[19] This fraction scales with the surface covered by the porous lithium film. Hence, a suitable first approximation for the lithium deposits is a solid film with a flat reactive surface. The surface area covered by this film is given by A_{Pl} and the thickness of the film is d_{Pl}. The change in the amount of plated lithium is given by a mass balance equation. The amount of plated lithium on the surface of graphite n_{Pl} changes over time as a function of the chemical intercalation ($Ch.Int.$) and the plating reaction (Pl/St)

$$\frac{\partial n_{\text{Pl}}}{\partial t} = \left(N_{\text{Ch.Int.}} - N_{\text{Pl/St}}\right) \cdot A_{\text{Pl}} \, . \tag{25}$$

The active surface for the chemical intercalation and lithium deposition is identical and given through A_{Pl}. The deposition of metallic lithium on the graphite surface in our model divided is in two different growth regimes. First, the interface between the graphite and the electrolyte is covered with plated lithium (increase of A_{Pl}). As soon as the surface element is completely covered ($A_{\text{Pl}} = A_{\text{Total}}$), further deposition of metallic lithium leads to an increase of thickness d_{Pl}. These growth regimes are indicated by arrows in Figure 1c).

The amount of metallic lithium on the graphite surface $n_{\text{Pl}}^{\text{Limit}}$ which prevents further

lithium intercalation is a parameter of our model and not easy to assess experimentally. In this study we assume, that the graphite surface is completely covered by plated lithium as soon as the amount of lithium n_{Pl} on the surface corresponds to a mono layer of metallic lithium $n_{\mathrm{Pl}}^{\mathrm{Limit}} = n_{\mathrm{Pl}}^{\mathrm{1ML}}$ (see Table S1).The surface area covered by plated lithium A_{Pl} is, therefore, expressed as function of the amount of plated lithium n_{Pl}

$$A_{\mathrm{Pl}} = \begin{cases} \frac{n_{\mathrm{Pl}}}{n_{\mathrm{Pl}}^{\mathrm{Limit}}} \cdot A_{\mathrm{Total}} & , \; n_{\mathrm{Pl}} < n_{\mathrm{Pl}}^{\mathrm{Limit}} \\ A_{\mathrm{Total}} & , \; otherwise \end{cases} . \tag{26}$$

The calculation of limiting Li surface deposits $n_{\mathrm{Pl}}^{\mathrm{Limit}}$ is presented in the supporting information (see Eq. S-4).The thickness of plated lithium d_{Pl} on top of a given surface A_{Total} is calculated from the amount of lithium needed to form one mono layer $n_{\mathrm{Li}}^{\mathrm{1ML}}$. The thickness of plated lithium is therefore related to the thickness of one mono layer of metallic lithium $d_{\mathrm{Li}}^{\mathrm{1ML}}$ through

$$d_{\mathrm{Pl}} = n_{\mathrm{Pl}} / n_{\mathrm{Li}}^{\mathrm{1ML}} \cdot d_{\mathrm{Li}}^{\mathrm{1ML}} . \tag{27}$$

The thickness of one mono layer of metallic lithium is given through the molar volume of lithium ν_{Li} and the Avogadro constant N_{A}: $D_{\mathrm{Li}}^{\mathrm{1ML}} = \sqrt[3]{\nu_{\mathrm{Li}} / N_{\mathrm{A}}}$ (See also Section (S-1) in the supporting information).

The uncovered surface $A_{\mathrm{Free}} = A_{\mathrm{Total}} - A_{\mathrm{Pl}}$ is given by the total graphite surface area reduced by the surface which is covered with plated lithium. In general the volume of intercalation electrodes changes with the state of charge (SoC), which affects the total surface area A_{Total}. For simplicity we assume, that the variation of total surface area can be neglected and the surface area is hence treated as a constant. The free and plated surface area is also indicated in Figure 1 b).

The proposed surface model including a description for lithium plating is coupled to mass and charge transport in the active material and liquid electrolyte. The governing equations and fluxes in the different phases are based on the theory of Latz *et al.*[30] and are defined in Table 1. The governing equations (see Table 1) are coupled at the interfaces between the phases under the assumption of a continuity of lithium and charge flux. In the case of pure lithium intercalation (I), these conditions can be written as

$$\vec{j}_{\mathrm{El}} \cdot \vec{n} = N_{\mathrm{Inter}} = \vec{j}_{\mathrm{So}} \cdot \vec{n} \tag{28}$$

$$\vec{N}_{\mathrm{El}} \cdot \vec{n} = j_{\mathrm{Inter}} = \vec{N}_{\mathrm{So}} \cdot \vec{n} \ , \tag{29}$$

with $\vec{n}$ the surface normal pointing from the solid into the electrolyte. The introduction of lithium plating and the corresponding surface reaction model (Eq. 1 - Eq. 3) lead to an extension of the interface conditions:

$$\vec{N}_{\mathrm{So}} \cdot \vec{n} = \frac{A_{\mathrm{Pl}}}{A_{\mathrm{Total}}} \cdot N_{\mathrm{Ch.Int.}} + \left(1 - \frac{A_{\mathrm{Pl}}}{A_{\mathrm{Total}}}\right) \cdot N_{\mathrm{Inter}} \tag{30}$$

$$\vec{N}_{\mathrm{El}} \cdot \vec{n} = \frac{A_{\mathrm{Pl}}}{A_{\mathrm{Total}}} \cdot N_{\mathrm{Pl/St}} + \left(1 - \frac{A_{\mathrm{Pl}}}{A_{\mathrm{Total}}}\right) \cdot N_{\mathrm{Inter}} \tag{31}$$

$$\vec{j}_{\mathrm{So}} \cdot \vec{n} = \frac{A_{\mathrm{Pl}}}{A_{\mathrm{Total}}} \cdot j_{\mathrm{Pl/St}} + \left(1 - \frac{A_{\mathrm{Pl}}}{A_{\mathrm{Total}}}\right) \cdot j_{\mathrm{Inter}} \tag{32}$$

$$\vec{j}_{\mathrm{El}} \cdot \vec{n} = \frac{A_{\mathrm{Pl}}}{A_{\mathrm{Total}}} \cdot j_{\mathrm{Pl/St}} + \left(1 - \frac{A_{\mathrm{Pl}}}{A_{\mathrm{Total}}}\right) \cdot j_{\mathrm{Inter}} \tag{33}$$

It is noteworthy, that the interface conditions for the lithium flux on the solid (Eq. 30) and electrolyte (Eq. 31) side are not symmetric, because the chemical intercalation $N_{\mathrm{Ch.Int.}}$ is charge neutral. The symmetry is preserved for the interface condition of the current flux (Eq. 32 and Eq. 33).

In the equations above we assume a homogeneous surface composition and neglect contributions of the SEI. The development of SEI models is a challenge itself and numerous approaches are published in the literature.[32,43,34] The model presented in this work can be readily extended to include the growth of SEI, as well as its effect on mass transport and kinetics on the electrode surface. However, a detailed description of the SEI is not in the focus of this work. Nevertheless, a first phenomenological treatment of the effect of the SEI properties on the occurrence of lithium plating events is presented in this work.

3 Results of electrochemical simulations

The presented model for lithium plating is independent of a transport model and can therefore be incorporated into different commonly used electrochemical models, such as homogenized approaches (Newman-type or single particle) or spatially resolved 3D simulations. In order to demonstrate the key features of the newly devised model we implemented it into the simulation framework BEST. More information about the numerical approaches, which are implemented in our framework, can be found in Ref. 44. With this tool we perform simulation studies on an artificial, yet realistic, 3D graphite microstructure (see Figure 2a)). First, we study the overcharge of homogeneous model electrodes. The impact of inhomogeneities in the electrode, introduced e.g. by the SEI, is investigated in the second part of the results section.

The model is parameterized in order to represent half-cells consisting of a graphite electrode, a polymer seperator, and a lithium metal counter electrode soaked with an electrolyte solution of 1M $LiPF_6$ in PC:EC:DMC.[45] A list of parameters can be found in the supporting information (see Table S2). The microstructural realization of the graphite electrode (see Figure 2a)) is constructed using Geodict[46] by piling convex polyhedrons, which creates a representative geometry similar to SEM images reported in the literature. This relatively simple approach provides a realistic representation of anode microstructures which is sufficient for

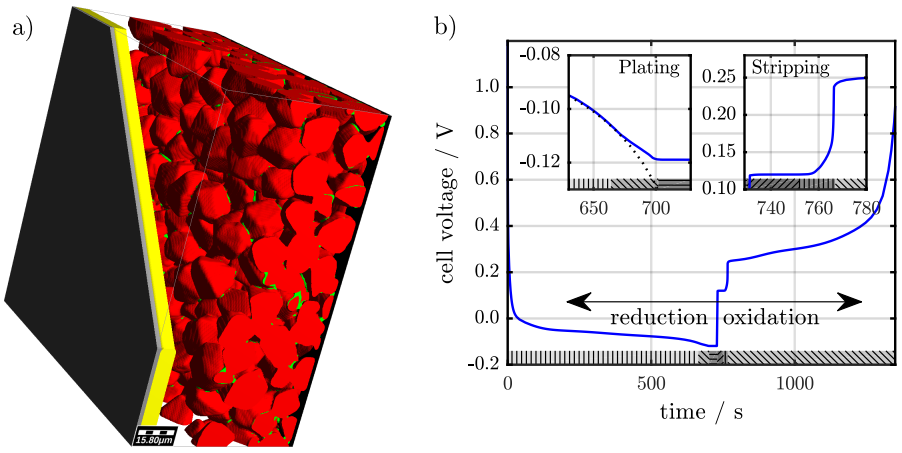

Figure 2: a) Visualization of the used electrode microstructure with currentcollector and counter electrode. The counter electrode is cut in the figure to reveal the seperator-graphite-interface. The porous electrode consists of graphite (red) and binder (green). b) The cell voltage of the lithiation-delithation simulations exhibits two voltage plateaus. The one at the end of lithiation indicates a fully plated electrode, while the one at the start of delithiation corresponds to the stripping of plated lithium. The cell voltage without plating is included as dotted line in the left inset.

the demonstration of our plating model. Other sources for more exact representations of graphite electrodes are tomography techniques[47] or sophisticated stochastic microstructure generators.[48] However, this is not in the focus of this work. The resulting graphite anode has a density of 1.17 g/cm^3. This corresponds to a porosity of 47.49 %, a solid volume fraction of graphite of 49.70 % and a small amount of inactive material of 2.81 %, which represents binder and conductive additive. The thickness in through direction is 51 μm. The overall simulation domain consists of 4160000 cubic voxels with a side length of 0.74 μm. This corresponds to 77 μm in *through direction*[49] and 148 μm in *lateral direction*.[50] The plating/stripping simulations were performed on the high performance cluster JUSTUS located at Ulm University.

3.1 Homogeneous electrochemical situation

In order to investigate lithum plating and stripping we simulate a constant current reduction/lithiation and oxidation/delithiation experiment, which is commonly used in abuse tests of lithium-ion battery anodes. The cell voltage of the simulation is shown in Figure 2b). Dur-

ing lithiation a total charge of 400 nAh, which corresponds to 1.83 mAh cm^{-2}, was transferred from the lithium counter electrode into graphite. The switch from lithiation to delithiation is taking place at $t = 730\,s$. For the subsequent delithiation we use a cut-off voltage of 1 V. The applied current of 90 A m^{-2} corresponds to roughly 5 C, which is close to the targets of the automotive industry regarding fast charging applications. The initial values for concentrations and potentials are listed in Table S3 in the supporting material.

During lithiation most of the cell voltage is below zero due to the high current density and resulting ohmic and kinetic losses. Six different regions are marked in Figure 2b) through hatched bars with gray background. These regions, from left to right, are refered to by the names of the dominating reactions: pure lithiation, simultaneous lithium plating and intercalation, pure lithium plating, lithium stripping, simultaneous lithium stripping and delithiation, and pure delithation. The lithiation of the graphite begins at $t = 0\,s$. In this first phase the cell voltage follows the shape of the graphite open-circuit potential (See Eq. S-5). Around $t = 664\,s$ we observe in our simulations small spots of lithium deposits on the electrode surface at different positions close to the separator. At the same time, the cell voltage of a simulation with plating deviates from the cell voltage of a simulation without the plating model (dashed line in left inset of Figure 2b)). The deposition of lithium continues until the complete surface of the graphite electrode is covered with metallic lithium. The complete coverage is indicated by the constant voltage plateau starting around $t = 702\,s$. In this state the battery cell effectively represents a flat lithium metal electrode with a porous lithium metal counter electrode. The transition from pure lithiation to a fully plated state clearly leads to a change in the slope of the cell voltage. The pure lithiation (representing normal battery operation) and the fully plated electrode (representing lithium-lithium cells) are established cases. The detection of the transition feature in the cell voltage could possibly be used to detect the onset of lithium plating during operation of a full cell. The constant value in the cell voltage was reported by Wandt *et al.*[11] for a constant current overcharge of a graphite electrode. By applying *operando* electron paramagnetic resonance

(EPR) spectroscopy Wandt *et al.* were able to correlate the constant voltage regions to the formation of a metallic lithium phase. In the simulations, the feature occurs during a constant current lithiation. Common charging protocols typically consist of a constant current phase followed by a step at constant voltage. If the onset of plating occurs during constant current, the analysis of the differential voltage (DV, dV/dQ vs Q) could be a suitable method for the detection of this plating signal. This technique is often used to investigate the degradation behavior of lithium-ion batteries.[3,51] The sensitivity of the differential voltage to the plating onset depends on the time resolution during the charging of a lithium-ion battery. The differential voltage for the simulation is presented in Figure 3a). The DV-signal exhibits the onset of lithium plating as a deviation from the graphite signal

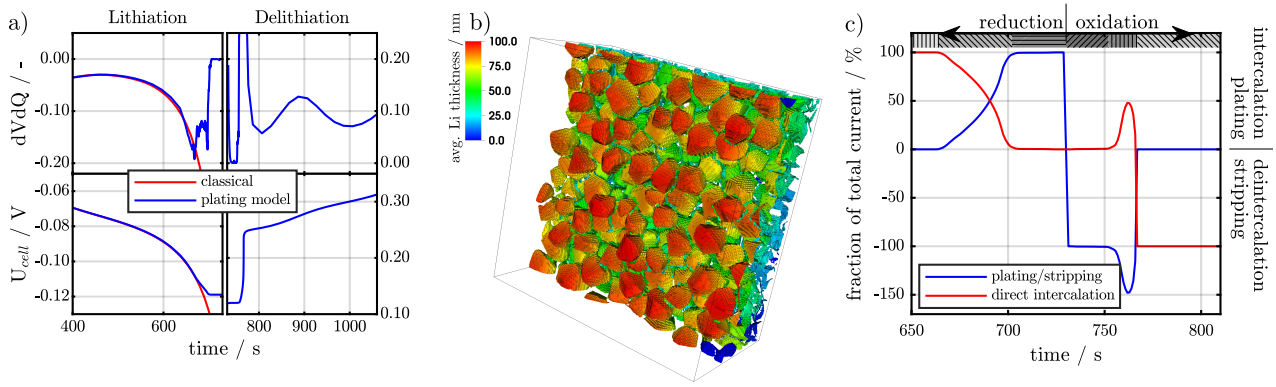

Figure 3: a) The differential voltage exhibits two features for the plating onset and the end of stripping. b) The spatial distribution of the average thickness of plated lithium for $t = 728.8\,\mathrm{s}$, as seen from the separator, exhibits a clear gradient from the separator towards the current collector. Some graphite particles show a larger thickness (dark red) than their surroundings. Additional images of the lithium distributions can be found in the supporting information. c) The contribution of the direct intercalation or plating/stripping reaction to the total current through the half-cell is shown.

and vanishes completely as soon as the complete surface is covered by metallic lithium. The detection of this feature during measurements strongly depends on time resolution and the charging protocol. Additionally, the open-circuit potential of the cathode will add complexity to the DV-signal. The stripping plateau during delithiation results in a peak in the differential voltage during delithiation at the end of lithium stripping. This peak is used as an indirect indicator for lithium plating.[3] Commonly, the anode has an excess capacity and the charge

protocols often switch from constant current towards constant voltage charging at a given cell voltage. This charging protocol might shift the plating onset into the constant voltage regime, thus preventing the detection as a voltage feature. The magnitude of the onset feature is proportional to the surface covered by plated lithium. Post-mortem analysis indicates, that lithium plating often occurs only locally.[52] If only a small fraction of the surface is covered, the feature in the cell voltage might be less pronounced. The current signal during constant voltage operation was studied by Schindler *et. al*[53] using a modified differential voltage method. They were able to correlate a feature in the current signal during the constant voltage phase with the existence of a stripping plateau during a subsequent cell relaxation. The presented plating model together with a thorough parameterization and dedicated full cell experiments will allow to investigate the detectability of the voltage feature. So far, the authors are not aware of any publication reporting a voltage feature in their measurements of lithium-ion batteries.

The spatial distribution of the plated lithium inside the 3D microstructure just before the switch from reduction to oxidation of the graphite can be seen in Figure 3b). The unconnected particle in the lower right corner at the separator interface exhibits no plated lithium, since it is electrochemically inactive. The plated lithium phase close to the current collector (back) is thinner than the region close to the separator interface (front). The spatial distribution as seen in Figure 3b) shows small inhomogeneities at the separator interface, where some particles have a thicker lithium film on the surface. The affected particles are slightly closer to the separator and are, thus, preferentially lithiated in the first stage. This favors lithium plating at an earlier stage during battery charge resulting in a slightly longer plating duration and increased thickness. Similar inhomogeneous distributions were seen experimentally by Harris *et al.*[6] using an optical microscope for *in situ* observations. It is suspected, that such local variations can affect SEI formation and, thus, promote locally enhanced Li plating in subsequent lithiation/delithiation cycles as discussed below.

The applied current is changed from lithiation to delithiation conditions at $t = 730\,\mathrm{s}$, as

a result we observe a jump in the cell voltage (see Figure 2 b)). At the start of this stage the cell voltage also exhibits a region of nearly constant voltage. The absolute cell voltage is the same as in the subsequent final phase under lithation condition, which is a feature of the pseudo-symmetrical Li electrode. This constant voltage phase during stripping is often called *stripping plateau*. In experiments this plateau is typically not completely flat[4,53–55] since the surface is most likely not fully covered with lithium and one has a superposition of lithium stripping and lithium de-/intercalation. It should be noted, that during constant voltage charging plated lithium can potentially be dissolved and a stripping plateau during subsequent discharge would not appear, thus, falsely indicating an unplated battery.[56] The correct identification of a stripping plateau within the differential voltage signal is not unambiguous, since the concentration dependence of the lithium diffusion inside the graphite can also lead to a similar feature in the cell voltage.[57] A decrease of the lithium diffusion coefficient inside graphite at large state of charge will probably enhance the deposition of metallic lithium. The effect of a concentration dependent and anisotropic diffusion coefficients will be addressed in future research.

In a previous study[58] we additionally found, that depending on the current density some metallic lithium actually dissolves in the electrolyte and intercalates in the graphite material in a superposed equilibration process. This effect is discussed in more detail in the following paragraph.

The total current flowing through the separator is equal to the current imposed on the battery. Therefore, the current flowing through the interface between the solid phase and the electrolyte has to be equal to the applied current. The contribution of the intercalation and the plating reaction to the total current is presented in Figure 3c). If the surface of the graphite is fully covered with metallic lithium, the transfer of charge between solid phase and electrolyte is only possible through the stripping and plating reaction. As soon as the metallic lithium is removed from part of the electrode surface, the intercalation and deintercalation reaction becomes active again. The intercalation reaction has a different

dependence on the electrochemical potentials (see Eq. 17) than the stripping reaction (see Eq. 20). The global charge conservation allows local intercalation of lithium ions, if the local overpotential (see Eq. 17) favors this process. The overall current through the interface will still be identical to the externally supplied current, which corresponds to a net deintercalation current or reduction of lithium. In the presented simulations, as soon as uncovered surface is available, the intercalation reaction starts to lead to a net intercalation around $t = 752\,\mathrm{s}$ (cf. Figure 3c)). Locally, intercalation and deintercalation can occur (see Figure S3d) in the supporting information). The current due to the stripping reaction increases at the same time so the overall current flowing through the interface between solid and electrolyte corresponds to the applied current. The concurrent stripping and intercalation in the graphite electrode form a kind of local current loops. The magnitude of these current loops depends on the ratio of plated to free surface, on the reaction rate constants $N^{00}_{\mathrm{Pl/St}}$ and N^{00}_{Inter}, and the applied external current. These localized current loops, which do not contribute to the net current flowing through the battery, are most likely the most prominent mechanism to remove plated lithium during discharge of a LIB. The cell voltage increases due to the superposition of the potential dependence of the lithium stripping and the intercalation reaction. After complete dissolution of the plated lithium (around 767 s) the cell voltage reverts to the pure constant current deintercalation voltage of graphite. Note, that the concurrent intercalation reaction enhances stripping of plated lithium. As a result, the metallic lithium phase is completely removed in 37 s, while the time spend under plating conditions is more than 65 s. The chemical intercalation reaction (see Eq. 3) has no visible effect on the cell voltage, since in this work it is assumed to be a slow reaction and, therefore, negligible for the high current operation shown here. Including a constant voltage phase at the end of the reduction simulation or a rest period between the reduction and oxidation will allow the chemical intercalation to shift some of the plated lithium into the supporting graphite. A longer rest period after charging reduce or completely removes the stripping plateau.[59,60]

In order to improve the interpretation of the voltage signal, the evolution of the plated

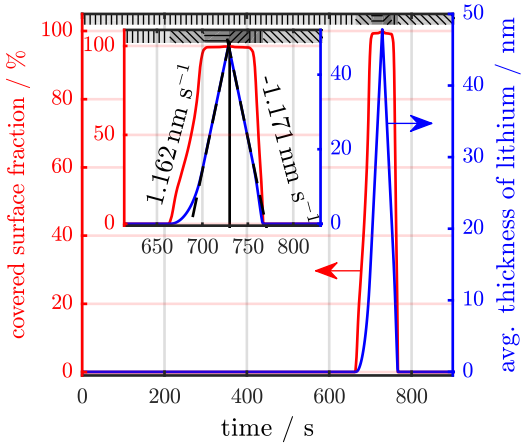

Figure 4: The average thickness of the plated lithium phase as a function of time shows an increase in plated lithium at the end of lithiation followed by a decrease and vanishing of plated lithium during delithiation. The inset shows a blow-up were the change from lithiation to delithiation is taking place

lithium phase will be discussed in more detail in this paragraph. The average thickness of plated lithium and the coverage of active surface is shown in Figure 4 as a function of time. The surface coverage is close to 100 per cent during lithium deposition. This indicates, that nearly the complete active surface is covered by plated lithium also taking into account unconnected particles (see lower right corner in Figure 3b)). The lithium thickness grows continuously during the deposition phase, since the majority of the applied current is driving the plating reaction. It takes around 35 s to completely cover the electrode surface. The average thickness is 47.85 nm, while the maximum thickness locally reaches up to 100 nm. The lithium thickness exhibits linear growth regions during plating and stripping. Two linear fits and their respective slopes are added in the inset of Figure 4. The deviation of the average thickness of lithium from the two lines indicates regions, where a significant fraction of the surface is not covered by plated lithium. During this phase both the plating/stripping reaction and lithium de-/intercalation have contributions to the total current (see Figure 3c)). Even after lithium plating is taking place locally at the separator interface, still a major part of the electrode allows for intercalation. The plating of lithium starts after around 670 s and intercalation close to the current collector continues until $\approx$ 700 s. A similar situation

is observed during the stripping process. The coexistence of fully plated and free surface regions gives rise to the afore mentioned current loops.

Additional images, which depict the spatial distribution of the plated lithium (see Figure S2) and the contribution of the intercalation and plating reaction to the current flow (see Figure S3) during lithium plating and striping (see Figure S1), can be found in the supporting material.

3.2 Influence of applied current

In this section we will touch on the detrimental effects of ultra-high charging rates. Figure 5 shows the cell voltage for two larger current densities. An increase of the applied current density leads to an earlier onset of lithium plating. At $9\,\mathrm{mA/cm^2}$ a charge of about

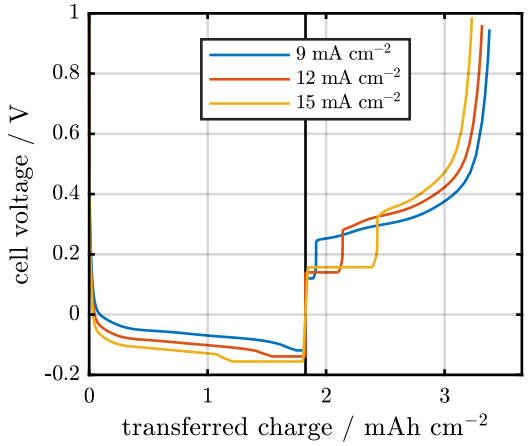

Figure 5: The cell voltage for the lithiation-delithiation with three different current densities

$1.6\,\mathrm{mAh/cm^2}$ can be transferred before plating starts. At the highest current of $15\,\mathrm{mA/cm^2}$ this capacity reduces to only $1.0\,\mathrm{mAh/cm^2}$. Thus, significantly more metallic lithium will be deposited on the graphite surface at higher currents. The earlier onset and the larger amount of plated lithium is visible in the supporting information in Figure S4, which displays the average thickness of plated lithium. Additionally, the local average of plated lithium in through direction as a function of time can be found in Figure S6 in the supporting infor-

mation. The start of lithium plating at the graphite-separator-interface is clearly visible. The thickness of the metallic lithium at the separator reaches an average thickness of over 500 nm. On this length scale the deposits might hinder the transport of lithium ions in the electrolyte. Blocked pores will prevent further deposition inside the electrode structure and enhance the lithium deposition on the electrode surface close to the separator. In our current model we do not take into account the effect of the lithium phase on electrode morphology or electrolyte transport. This is work in progress and an interesting aspect for future research.

In Figure 6 the average state of charge for the graphite surface close to the separator, close to the current collector and over the complete surface is presented. The surface close

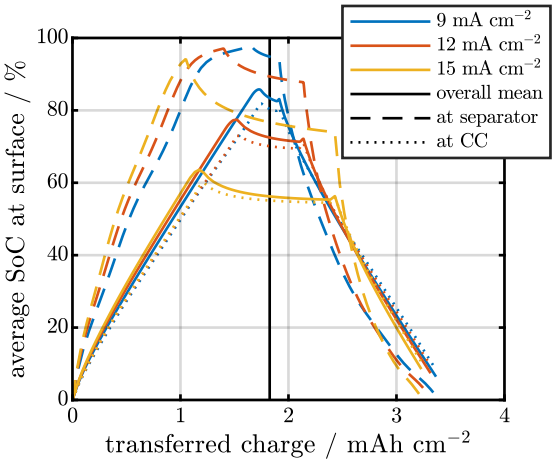

Figure 6: The average state of charge of the graphite surface for the three currents close to the separator, close to the current collector and the overall average value. An increase of the applied current enhances the spread of SoC between separator and current collector

to the separator exhibits a significantly higher state of charge during lithation compared to the region close to the current collector. The SoC at the separator surface increases faster for higher currents. Thus, the deposition of metallic lithium at the surface becomes thermodynamically favorable at lower transferred charges compared to the lowest current. Figure S7 presents the state of charge averaged over the complete surface, the complete electrode and the part without the surface. It can be seen, that the inner part of the electrode exhibits a lower state of charge due to the slow process of lithium diffusion. No

direct intercalation can take place as soon as the complete surface is covered with plated lithium. Therefore, the spread of the state of charge between the inner and the surface part reduces due to the diffusion of lithium.

Note, that decreasing the temperature of the LIB will have a similar effect on battery performance. The lithium diffusion coefficient in graphite reduces for decreasing temperature. This leads to the accumulation of lithium close to the surface of graphite. Similar effects will be observed at high currents (cf. Figure S7). The intercalation and lithium plating reactions will be slower with decreasing temperature. Thus, a larger potential drop will occur at the graphite-electrolyte-interface, which generally favor earlier lithium deposition. These two processes, together with other interfacial heating sources, such as the irreversible Joule heating or the reversible Peltier effect, can introduce local temperature inhomogeneities.[30,61] Thus adding another level of complexity to the parametrization and simulation. The combination of the plating model and thermal simulations is an interesting research topic in itself.

3.3 Influence of inhomogeneous SEI

Post-mortem analysis of cycled graphite electrodes often reveals inhomogeneous degradation and lithium deposition at the separator interface of the electrode.[5,52] Besides lithium plating continued growth of the solid-electrolyte-interphase (SEI) is a major degradation process at the electrode surface. This SEI on the surface of graphite has a large impact on the lifetime of lithium-ion batteries since the production of SEI irreversible consumes lithium and electrolyte. Additionally, the SEI hinders the intercalation reaction. Under extreme conditions the growth of SEI can also severely hinder the transport in the pore space. Experimentally both inhomogeneous SEI growth and lithium plating are observed. Both topics are a subject to our ongoing research. One possible source is the crystal structure of graphite itself, which consists of graphene layers.[62] This layered structure leads to an anisotropic diffusion of lithium. At the surface of the graphite particles, the orientation of the graphene planes

with respect to the interface affects the intercalation reaction.[63] Both effects can be included in our model. Additionally, including a model for SEI growth will allow for the prediction of the degradation behavior of lithium-ion batteries during cycling and storage.[34] A first study shedding some light on the influence of inhomogeneous SEI on lithium plating will be presented in the following paragraph. Hence, in the remainder of this chapter we will focus on the effect of inhomogeneous surface properties e.g. due to non-uniform SEI formation. The SEI influences the reactions at the interface between graphite and electrolyte through an additional potential drop over its thickness due to low ionic and electronic conductivity. The resulting resistance is commonly introduced as current dependent term in the overpotential[20]

$$\eta_{\text{w SEI}} = \eta_{\text{w/o SEI}} - j \cdot R_{\text{SEI}} \ , \tag{34}$$

where j is the current through the SEI between electrolyte and graphite and R_{SEI} a resistance due to the thickness of the SEI. The resistance R_{SEI} is assumed to depend on the SEI thickness d_{SEI} and the conductivity of the SEI σ_{SEI}

$$R_{\text{SEI}} = \frac{d_{\text{SEI}}}{\sigma_{\text{SEI}}} \ . \tag{35}$$

During lithiation the overpotential $\eta_{\text{w SEI}}$ is below zero and the expression for the exchange current density (see Eq. 4) can be approximated to

$$N_i^{\text{w SEI}} \approx -\frac{N_i^0}{\exp\left[(1-\alpha)\beta \cdot |j| \cdot R_{\text{SEI}}\right]} \cdot \exp\left[-(1-\alpha)\beta\eta_i^{\text{w/o SEI}}\right] \ , \tag{36}$$

with $\beta = F/RT$ and $|j|$ the absolute value of the current flux of reaction i as given by $j = N_i \cdot F$. A more detailed explanation of the assumptions of this approximation can be found

in the supporting information. The reaction rate constant N_i^{00} and the SEI contribution in Eq. 36 are merged into the modified rate constant $N_i^{00,mod}$. The rate constant for the intercalation reaction through a SEI can therefore be expressed as follows

$$\begin{aligned} N_{\text{Inter}}^{0,mod} &= \frac{N_{\text{Inter}}^{00}}{\exp\left[\frac{0.5\ F}{R\ T} \cdot |j_{\text{Inter}}| \cdot R_{\text{SEI}}\right]} \cdot \sqrt{c_{\text{El}} \cdot c_{\text{So}}} \\ &= N_{\text{Inter}}^{00,mod} \cdot \sqrt{c_{\text{El}} \cdot c_{\text{So}}}\ . \end{aligned} \tag{37}$$

The modified reaction rate $N_{\text{Inter}}^{00,mod}$ depends on the local SEI resistance R_{SEI} and therefore on the local thickness of the SEI d_{SEI}. The influence of local variation of the SEI thickness on the lithium plating can therefore be investigated through a local variation of the modified reaction rate constant. In this work we use a simple model geometry to highlight the effect of local variations in SEI thickness. The porous electrode is split into two regions with locally varying reaction rate. The two regions are highlighted in Figure 7 by blue and red color, respectively. In the two regions, the interfacial area between the active material and the

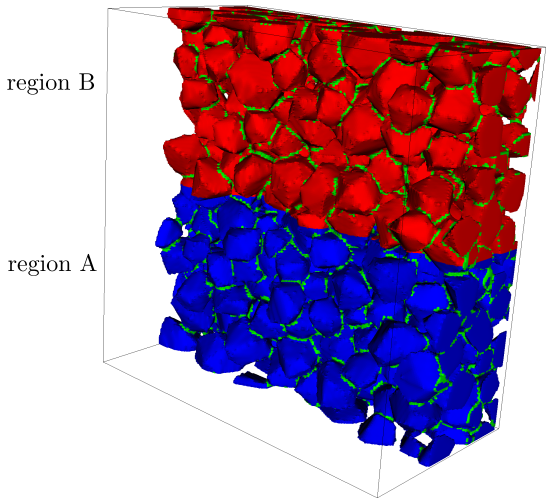

Figure 7: The microstructure of the graphite is split into two regions, marked by blue (region A) and red (region B), which have an identical active surface area

electrolyte have nearly the same size. The reaction rate constant in region B is reduced by one order of magnitude with respect to the value in region A, thus, mimicking a higher SEI

thickness. With a conductivity of the SEI in the order of $3.4 \cdot 10^{-7}\,\mathrm{S/m}$,[32] the difference in N_{Inter} corresponds to approximately 5 nm difference in SEI thickness. This highlights that a fluctuation of the SEI thickness of some nanometers can significantly influence the intercalation kinetics. The resulting cell voltage for simulations with homogeneous and

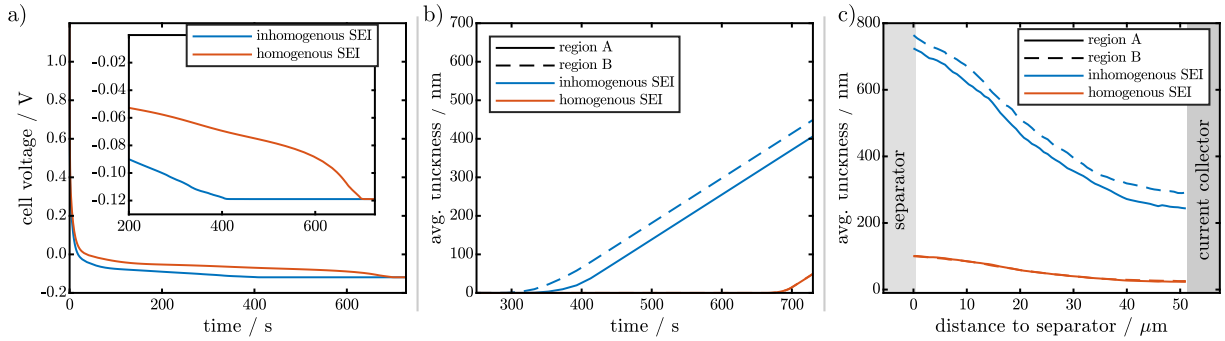

Figure 8: a) The cell voltage for the inhomogeneous and homogeneous SEI thickness exhibit different behavior. A thicker SEI in region B leads to an early onset of a constant voltage region, which indicates lithium plating. b) The average thickness of plated lithium for the two cases and regions is shown. A thicker SEI in region B leads to earlier deposition of lithium. c) The average thickness of plated lithium at $t \approx 730\,\mathrm{s}$ in through direction is shown. The largest deposition of lithium always occurs at the separator side of the electrode. The plated Lithium is thicker in region B for inhomogeneous case.

inhomogeneous SEI is presented in Figure 8a). In the inhomogeneous case region B has a lower kinetic factor representing a thicker SEI. The corresponding simulation exhibits larger overpotential and reaches the constant plateau associated with complete coverage of the surface with plated lithium faster than the homogeneous case. The start of lithium plating and its temporal evolution can be seen in Figure 8b), where the average thickness of plated lithium inside the two regions is extracted from the spatial simulation output. The thicker SEI in region B leads to a larger amount of plated lithium in that region. Analyzing the spatial distributions of the plated lithium at different time steps reveals, that lithium deposition first occurs at the separator interface of region B. Then it continues mainly in the porous electrode in region B. Additional images depicting the spatial distributions of the plated lithium for different time steps and selected SEI thicknesses can be found in the supporting information (see Figure S8). The surface of region A is then slowly plated

with lithium at the separator interface with the highest deposition at the border to region B. The average spatial distribution through the electrode thickness at the end of lithiation ($t = 730\,\mathrm{s}$) is presented in Figure 8c). The thickest layer of plated lithium is close to the separator for both cases and regions.

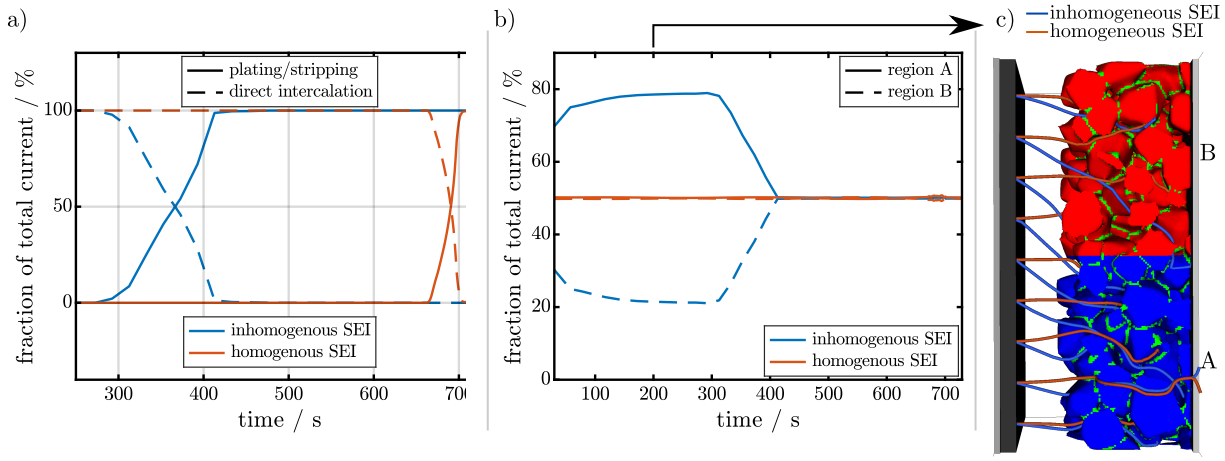

Figure 9: a) The switch of intercalation to plating as major charge transferring reaction is shown for the homogeneous and inhomogeneous SEI. The change occurs the quickest for the homogeneous case. b) A thicker SEI in region B leads to an increased current flux through the surface of region A until the surface is complete covered with metallic lithium. c) The path of the current for two cases at $t \approx 200\,\mathrm{s}$. The two regions are colored identically to Figure 7.

The contribution of the plating or the intercalation reaction to the local interface current is shown in Figure 9a) as function of time for the two case. Initially, the intercalation reaction is the major charge transfer reaction at the graphite-electrolyte-interface. The onset of lithium plating is clearly visible, when the plating reaction starts to contribute to the total current. A homogeneous SEI leads to a fast transition from an intercalation dominated current to plating dominated current. A locally inhomogeneous SEI causes a longer transition period between intercalation and plating dominated charge transfer. In the presented case the transition takes almost three times longer. The contribution of the interface current in each region to the total current reveals an imbalance of the local current for the inhomogeneous SEI (see Figure 9b)). However, we do not observe significant differences between the two regions for the homogeneous case. Each region contributes with 50 % to the total current.

For the inhomogeneous SEI the majority of the charge transfer between electrolyte and graphite occurs in region A. Starting at the onset of lithium plating, the contributions of the two regions to the total current start to equalize. The increased current in region A for the inhomogeneous SEI is mostly due to the intercalation reaction. The exact contribution of the intercalation and plating reaction in each region is presented in Figure S9 in the supporting information. There it is apparent, that region B reaches complete coverage of the surface faster than region A since the intercalation current in that region vanishes earlier than in region A. The focus of intercalation in region A leads to a significant difference in the lithiation of the graphite in the two regions. The graphite surface of region A reaches an average state of charge of 72 %, while the graphite surface in region B only increases until 20 % (see Figure S9c)). This vast difference in state of charge can lead to increased mechanical stresses between the two regions. Which, in turn, amplifies the inhomogeneous degradation of such an electrode.

In Figure 9c) the path of the current flow at nine selected locations for the two cases are superimposed into the 3D spatial microstructure. The microstructure is again divided into the two regions – region A (blue) and region B (red). The binder region is shown in green color. The current path is extracted from the spatial simulation results at around $t \approx 200\,\mathrm{s}$. The graphite electrode was cropped to improve the visibility. The current path is colored according to Figure 9b) (inhomogeneous SEI in blue and homogeneous SEI in red). In the homogeneous case the current stream lines follow the shortest path from the counter electrode to the graphite electrode. For the inhomogeneous SEI all paths are aligned towards the region A. This visually highlights the focus of the current due to the inhomogeneous SEI distribution.

The thicker SEI seems to have a similar impact on the cell voltage and the onset of the constant voltage phase during plating as the increase of the applied current for a homogeneous SEI as shown in Figure 5. It is probable, that an higher current density together with inhomogeneities in the SEI might exhibit an even larger impact on the localization of lithium

plating. The impact of SEI properties is rather complex and different plating behavior can arise depending on the e.g. SEI thickness corresponding to a state of health of the battery This highlights the need for improved models providing a coupled description of SEI growth and Li plating.

4 Summary and Conclusions

In this article we present a surface model of a graphite negative electrode describing lithium plating, charge neutral intercalation of plated lithium and intercalation. Therefore, we specifically take into account local competition between the different processes. The model is implemented in the simulation framework for spatially resolved simulations of lithium-ion batteries BEST. This enables the investigation of the effect of inhomogeneous microstructures on the plating and degradation behavior. Moreover our simulations give access to the spatial distribution of the lithium phase and allow correlations between lithium deposition and features in the electrochemical data. In addition to the well-known stripping plateau after lithium plating, our simulations predict a feature in the cell voltage at the onset of lithium plating. Further studies of this feature might enable its use for the detection of the onset of lithium plating similar to the feature in the current signal as investigated by Schindler *et. al.*[53]

Additionally, we make use of the spatial resolution of our approach and investigate the influence of local variations in the thickness of the SEI. An inhomogeneous SEI thickness favors localized lithium plating and can also lead to inhomogeneous lithiation of the graphite material. The difference of the overpotential of the plating reaction η_{PLEL} reveals, that lithium deposition starts in that region, which has the lower/more negative value (see Figure S11 in the supporting material).

A systematic study and parametrization is crucial to enable predictive simulations of lithium plating. Furthermore, the presented model can be extended to allow for concurrent

SEI growth at the plated lithium-electrolyte-interface[33,64] and the inclusion of electrochemical double layers.[65,66] The combination of these models with advanced characterization techniques will provide a valuable tool to study the growth mechanisms of metallic lithium and SEI during battery operation. This is of tremendous importance for the development of fast charging protocols.

5 List of symbols

The definition of the subscripts and superscripts can be found in Table 2. The definition of

Table 2: The subscript p indicates a phase, r a reaction and s a species.

Phase p		Reaction r		Species s	
So	solid/active material	$Inter$	direct intercalation	Li^+	Lithium ion
El	electrolyte	Pl/St	plating/stripping	Li^0 or Li	Lithium atom
Pl	plated lithium	$Ch.Int.$	chemical intercalation	e^-	Electron

the different parameters and symbols used in this manuscript can be found in Table 3.

Table 3: Parameters and their meaning

$\vec{j}_\mathrm{p}$	current flux density in p	$\vec{N}_\mathrm{p}$	lithium flux density in p
μ_s^p	chemical potential of s in p	μ_p	chemical potential of lithium in p
Φ^p	electrical potential in p		
$\tilde{\mu}_s^p$	electrochemical potential of s in p	φ_p	electrochemical potential of lithium in p
$\nu_{r,s}$	stoichiometric coefficient	a_s^p	activity of s in p
c_i^p	concentration of i in p	c_p	concentration of lithium
$c_i^{p,0}$	reference concentration of i in p	$c_\mathrm{p}^\mathrm{max}$	maximal lithium concentration
U_0	open-circuit potential		
D_p	diffusion coefficient of lithium	σ_p/κ_p	electronic/ionic conductivity in p
$t_\pm$	transference number	$f_\pm$	activity coefficient
j_r	areal current flux	N_r	areal lithium flux
ΔG_r	Gibbs free energy of reaction r	η_r	overpotential of reaction r
α_r	symmetry factor of reaction r		
N_r^0	pre-exponential factor	N_r^{00}	reaction rate constant
K_r^{00}	equilibrium constant of r		
n_Pl	amount of substance of plated lithium	$n_{Pl,0}$	phenomenological model parameter
$n_\mathrm{Pl}^\mathrm{Limit}$	amount of substance for complete coverage	$n_\mathrm{Pl}^\mathrm{1ML}$	amount of substance in one mono layer
d_Li	thickness of plated lithium	$d_\mathrm{Li}^\mathrm{1ML}$	thickness of one mono layer
A_{Total}	surface area of graphite	A_{Pl}	surface area covered by plated lithium
A_{Free}	surface area free of plated lithium		
$\vec{n}$	surface normal of area A between two phases		
T	temperature	R	Universal gas constant
F	Faraday constant	N_A	Avogadro constant
R_SEI	Resistance of SEI layer	σ_SEI	conductivity of SEI layer
d_SEI	thickness of SEI layer		
$\eta_\mathrm{w\ SEI}$	overpotential with existing SEI	$\eta_\mathrm{w/o\ SEI}$	overpotential without SEI contribution

Acknowledgement

The authors acknowledge support by the state of Baden-Württemberg through bwHPC and the German Research Foundation (DFG) through grant no INST 40/467-1 FUGG (JUSTUS cluster). This work contributes to the research performed at CELEST (Center for Electrochemical Energy Storage Ulm-Karlsruhe).

Supporting Information Available

The following files are available free of charge.

- ACS_AEM_SupportingInfo_Plating.pdf: Electrochemical Parameters, additional calculations, additional figures or the homogeneous electrochemical situation and for the inhomogeneous SEI

References

(1) Waldmann, T.; Hogg, B.-I.; Wohlfahrt-Mehrens, M. Li plating as unwanted side reaction in commercial Li-ion cells - A review. *J. Power Sources* **2018**, *384*, 107–124.

(2) Burns, J. C.; Stevens, D. A.; Dahn, J. R. In-Situ Detection of Lithium Plating Using High Precision Coulometry. *J. Electrochem. Soc.* **2015**, *162*, A959–A964.

(3) Petzl, M.; Kasper, M.; Danzer, M. A. Lithium plating in a commercial lithium-ion battery - A low-temperature aging study. *J. Power Sources* **2014**, *275*, 799–807.

(4) Petzl, M.; Danzer, M. A. Nondestructive detection, characterization, and quantification of lithium plating in commercial lithium-ion batteries. *J. Power Sources* **2014**, *254*, 80–87.

(5) Krämer, Y.; Birkenmaier, C.; Feinauer, J.; Hintennach, A.; Bender, C. L.; Meiler, M.; Schmidt, V.; Dinnebier, R. E.; Schleid, T. A New Method for Quantitative Marking of

Deposited Lithium by Chemical Treatment on Graphite Anodes in Lithium-Ion Cells. *Chem. - A Eur. J.* **2015**, *21*, 6062–6065.

(6) Harris, S. J.; Timmons, A.; Baker, D. R.; Monroe, C. Direct in situ measurements of Li transport in Li-ion battery negative electrodes. *Chem. Phys. Lett.* **2010**, *485*, 265–274.

(7) Yamaki, J.-I.; Tobishima, S.-I.; Hayashi, K.; Nemoto, Y.; Arakawa, M. A consideration of the morphology of electrochemically deposited lithium in an organic electrolyte. *J. Power Sources* **1998**, *74*, 219–227.

(8) Gireaud, L.; Grugeon, S.; Laruelle, S.; Yrieix, B.; Tarascon, J.-M. Lithium metal stripping/plating mechanisms studies: A metallurgical approach. *Electrochem. commun.* **2006**, *8*, 1639–1649.

(9) Bhattacharyya, R.; Key, B.; Chen, H.; Best, A. S.; Hollenkamp, A. F.; Grey, C. P. In situ NMR observation of the formation of metallic lithium microstructures in lithium batteries. *Nat. Mater.* **2010**, *9*, 504–10.

(10) Chang, H. J.; Trease, N. M.; Ilott, A. J.; Zeng, D.; Du, L. S.; Jerschow, A.; Grey, C. P. Investigating Li Microstructure Formation on Li Anodes for Lithium Batteries by in Situ 6Li/7Li NMR and SEM. *J. Phys. Chem. C* **2015**, *119*, 16443–16451.

(11) Wandt, J.; Jakes, P.; Granwehr, J.; Eichel, R.-A.; Gasteiger, H. A. Quantitative and time-resolved detection of lithium plating on graphite anodes in lithium ion batteries. *Mater. Today* **2018**, *21*, 231–240.

(12) Chen, K.-H.; Wood, K. N.; Kazyak, E.; LePage, W. S.; Davis, A. L.; Sanchez, A. J.; Dasgupta, N. P. Dead lithium: mass transport effects on voltage, capacity, and failure of lithium metal anodes. *J. Mater. Chem. A* **2017**, *5*, 11671–11681.

(13) Chazalviel, J.-N. Electrochemical aspects of the generation of ramified metallic electrodeposits. *Phys. Rev. A* **1990**, *42*, 7355–7367.

(14) Ward Jones, S. E.; Chevallier, F. G.; Paddon, C. A.; Compton, R. G. General theory of cathodic and anodic stripping voltammetry at solid electrodes: Mathematical modeling and numerical simulations. *Anal. Chem.* **2007**, *79*, 4110–4119.

(15) Skitał, P. M.; Sanecki, P. T. The experimental verification of mathematical two-plate model describing the metal deposition/dissolution process. *Russ. J. Electrochem.* **2012**, *48*, 797–803.

(16) Monroe, C. W.; Newman, J. Dendrite Growth in Lithium/Polymer Systems. *J. Electrochem. Soc.* **2003**, *150*, A1377–A1384.

(17) Jana, A.; Ely, D. R.; García, R. E. Dendrite-separator interactions in lithium-based batteries. *J. Power Sources* **2015**, *275*, 912–921.

(18) Rosso, M.; Chassaing, E.; Fleury, V.; Chazalviel, J.-N. Shape evolution of metals electrodeposited from binary electrolytes. *Journal of Electroanalytical Chemistry* **2003**, *559*, 165–173.

(19) Tan, J.; Ryan, E. M. Computational study of electro-convection effects on dendrite growth in batteries. *J. Power Sources* **2016**, *323*, 67–77.

(20) Arora, P.; Doyle, M.; White, R. E. Mathematical Modeling of the Lithium Depotision Overcharge Reaction in Lithium-Ion Batteries Using Carbon-Based Negative Electrodes. *J. Electrochem. Soc.* **1999**, *146*, 3543–3553.

(21) Doyle, M.; Newman, J.; Gozdz, A. S.; Schmutz, C. N.; Tarascon, J.-M. Comparison of Modeling Predictions with Experimental Data from Plastic Lithium Ion Cells. *J. Electrochem. Soc.* **1996**, *143*, 1890.

(22) Tippmann, S.; Walper, D.; Balboa, L.; Spier, B.; Bessler, W. G. Low-temperature charging of lithium-ion cells part I: Electrochemical modeling and experimental investigation of degradation behavior. *J. Power Sources* **2014**, *252*, 305–316.

(23) Tang, M.; Albertus, P.; Newman, J. Two-Dimensional Modeling of Lithium Deposition during Cell Charging. *J. Electrochem. Soc.* **2009**, *156*, A390–A399.

(24) Yang, X.-G.; Leng, Y.; Zhang, G.; Ge, S.; Wang, C.-Y. Modeling of lithium plating induced aging of lithium-ion batteries: Transition from linear to nonlinear aging. *Journal of Power Sources* **2017**, *360*, 28–40.

(25) Yang, X.-G.; Ge, S.; Liu, T.; Leng, Y.; Wang, C.-Y. A look into the voltage plateau signal for detection and quantification of lithium plating in lithium-ion cells. *Journal of Power Sources* **2018**, *395*, 251 – 261.

(26) von Lüders, C.; Keil, J.; Webersberger, M.; Jossen, A. Modeling of lithium plating and lithium stripping in lithium-ion batteries. *Journal of Power Sources* **2019**, *414*, 41–47.

(27) Harris, S. J.; Lu, P. Effects of inhomogeneities -Nanoscale to mesoscale -on the durability of Li-ion batteries. *Journal of Physical Chemistry C* **2013**, *117*, 6481–6492.

(28) Baker, D. R.; Verbrugge, M. W. Modeling Overcharge at Graphite Electrodes: Plating and Dissolution of Lithium. *Journal of The Electrochemical Society* **2020**, *167*, 013504.

(29) Latz, A.; Zausch, J. Thermodynamic consistent transport theory of Li-ion batteries. *J. Power Sources* **2011**, *196*, 3296–3302.

(30) Latz, A.; Zausch, J. Multiscale modeling of lithium ion batteries: thermal aspects. *Beilstein J. Nanotechnol.* **2015**, *6*, 987–1007.

(31) Fraunhofer Institute for Industrial Mathematics (ITWM), BEST - Battery and Electrochemistry Simulation Tool. `https://www.itwm.fraunhofer.de/best`, Accessed: 2019-09-13.

(32) Single, F.; Horstmann, B.; Latz, A. Revealing SEI Morphology: In-Depth Analysis of a Modeling Approach. *J. Electrochem. Soc.* **2017**, *164*, E3132–E3145.

(33) Single, F.; Latz, A.; Horstmann, B. Identifying the Mechanism of Continued SEI Growth. *ChemSusChem* **2018**, 1–7.

(34) von Kolzenberg, L.; Latz, A.; Horstmann, B. SolidâĂŘElectrolyte Interphase During Battery Cycling: Theory of Growth Regimes. *ChemSusChem* **2020**, 1–11.

(35) Latz, A.; Zausch, J. Thermodynamic derivation of a Butler-Volmer model for intercalation in Li-ion batteries. *Electrochim. Acta* **2013**, *110*, 358–362.

(36) Bazant, M. Z. Theory of Chemical Kinetics and Charge Transfer based on Nonequilibrium Thermodynamics. *Acc. Chem. Res.* **2013**, *46*, 1144–1160.

(37) Job, G.; Herrmann, F. Chemical potential - a quantity in search of recognition. *Eur. J. Phys.* **2006**, *27*, 353–371.

(38) Newman, J.; Thomas-Alyea, K. E. *Electrochemical systems*, 3rd ed.; John Wiley & Sons, 2004.

(39) Chen, C. F.; Mukherjee, P. P. Probing the morphological influence on solid electrolyte interphase and impedance response in intercalation electrodes. *Phys. Chem. Chem. Phys.* **2015**, *17*, 9812–9827.

(40) Barai, P.; Higa, K.; Srinivasan, V. Lithium dendrite growth mechanisms in polymer electrolytes and prevention strategies. *Phys. Chem. Chem. Phys.* **2017**, *19*, 20493–20505.

(41) Meibuhr, S. G. Electrode Studies in Nonaqueous Electrolytes. *J. Electrochem. Soc.* **1970**, *117*, 56–60.

(42) The sign convention of the ionic flux density N_i is such, that a negative value corresponds to a flux from the left side of the reactions (see Eq. 1, Eq. 2 and Eq. 3) towards the right side.

(43) Vetter, J.; Novák, P.; Wagner, M. R.; Veit, C.; Möller, K.-C.; Besenhard, J. O.; Winter, M.; Wohlfahrt-Mehrens, M.; Vogler, C.; Hammouche, A. Ageing mechanisms in lithium-ion batteries. *J. Power Sources* **2005**, *147*, 269–281.

(44) Hein, S. Modeling of lithium plating in lithium-ion-batteries. Ph.D. thesis, University Ulm, 2018.

(45) Valøen, L. O.; Reimers, J. N. Transport Properties of LiPF6-Based Li-Ion Battery Electrolytes. *Journal of The Electrochemical Society* **2005**, *152*, A882.

(46) Math2Market, GeoDict. `https://www.geodict.com/`, Accessed: 2019-09-13.

(47) Mitsch, T.; Krämer, Y.; Feinauer, J.; Gaiselmann, G.; Markötter, H.; Manke, I.; Hintennach, A.; Schmidt, V. Preparation and Characterization of Li-ion Graphite Anodes using Synchrotron Tomography. *Materials (Basel).* **2014**, 1–21.

(48) Feinauer, J.; Brereton, T.; Spettl, A.; Weber, M.; Manke, I.; Schmidt, V. Stochastic 3D modeling of the microstructure of lithium-ion battery anodes via Gaussian random fields on the sphere. *Comput. Mater. Sci.* **2015**, *109*, 137–146.

(49) The through direction is defined from negative towards positive current collector.

(50) The lateral direction is perpendicular to the through direction and therefore parallel to the current collector.

(51) Bloom, I.; Jansen, A. N.; Abraham, D. P.; Knuth, J.; Jones, S. A.; Battaglia, V. S.; Henriksen, G. L. Differential voltage analyses of high-power, lithium-ion cells 1. Technique and application. *J. Power Sources* **2005**, *139*, 295–303.

(52) Ghanbari, N.; Waldmann, T.; Kasper, M.; Axmann, P.; Wohlfahrt-Mehrens, M. Inhomogeneous Degradation of Graphite Anodes in Li-Ion Cells: A Postmortem Study Using Glow Discharge Optical Emission Spectroscopy (GD-OES). *J. Phys. Chem. C* **2016**, *120*, 22225–22234.

(53) Schindler, S.; Bauer, M.; Petzl, M.; Danzer, M. A. Voltage relaxation and impedance spectroscopy as in-operando methods for the detection of lithium plating on graphitic anodes in commercial lithium-ion cells. *J. Power Sources* **2016**, *304*, 170–180.

(54) Smart, M. C.; Ratnakumar, B. V. Effects of Electrolyte Composition on Lithium Plating in Lithium-Ion Cells. *J. Electrochem. Soc.* **2011**, *158*, A379–A389.

(55) Jones, J.-P.; Smart, M. C.; Krause, F. C.; Bugga, R. V. The Effect of Electrolyte Additives upon Lithium Plating during Low Temperature Charging of Graphite-LiNiCoAlO 2 Lithium-Ion Three Electrode Cells . *Journal of The Electrochemical Society* **2020**, *167*, 020536.

(56) Campbell, I. D.; Marzook, M.; Marinescu, M.; Offer, G. J. How observable is lithium plating? differential voltage analysis to identify and quantify lithium plating following fast charging of cold lithium-ion batteries. *Journal of the Electrochemical Society* **2019**, *166*, A725–A739.

(57) O'Kane, S. E. J.; Campbell, I. D.; Marzook, M. W. J.; Offer, G. J.; Marinescu, M. Physical origin of the differential voltage minimum associated with lithium plating in Li-ion batteries. *Journal of the Electrochemical Society* **2020**,

(58) Hein, S.; Latz, A. Influence of local lithium metal deposition in 3D microstructures on local and global behavior of Lithium-ion batteries. *Electrochim. Acta* **2016**, *201*, 354–365.

(59) Zinth, V.; von Lüders, C.; Hofmann, M.; Hattendorff, J.; Buchberger, I.; Erhard, S.; Rebelo-Kornmeier, J.; Jossen, A.; Gilles, R. Lithium plating in lithium-ion batteries at sub-ambient temperatures investigated by in situ neutron diffraction. *J. Power Sources* **2014**, *271*, 152–159.

(60) Zinth, V.; von Lüders, C.; Wilhelm, J.; Erhard, S. V.; Hofmann, M.; Seidlmayer, S.; Rebelo-Kornmeier, J.; Gan, W.; Jossen, A.; Gilles, R. Inhomogeneity and relaxation

phenomena in the graphite anode of a lithium-ion battery probed by in situ neutron diffraction. *J. Power Sources* **2017**, *361*, 54–60.

(61) Angeles Cabañero, M.; Altmann, J.; Gold, L.; Boaretto, N.; Müller, J.; Hein, S.; Zausch, J.; Kallo, J.; Latz, A.; Cabañero, M. A.; Altmann, J.; Gold, L.; Boaretto, N.; Müller, J.; Hein, S.; Zausch, J.; Kallo, J.; Latz, A. Investigation of the temperature dependence of lithium plating onset conditions in commercial Li-ion batteries. *Energy* **2019**, *171*, 1217–1228.

(62) Gallagher, K. G.; Dees, D. W.; Jansen, A. N.; Abraham, D. P.; Kang, S.-H. A Volume Averaged Approach to the Numerical Modeling of Phase-Transition Intercalation Electrodes Presented for LixC6. *J. Electrochem. Soc.* **2012**, *159*, A2029–A2037.

(63) Harris, S. J.; Rahani, E. K.; Shenoy, V. B. Direct In Situ Observation and Numerical Simulations of Non-Shrinking-Core Behavior in an MCMB Graphite Composite Electrode. *Journal of the Electrochemical Society* **2012**, *159*, A1501–A1507.

(64) Single, F.; Horstmann, B.; Latz, A. Dynamics and morphology of solid electrolyte interphase (SEI). *Phys. Chem. Chem. Phys.* **2016**, *18*, 17810–17814.

(65) Lück, J.; Latz, A. Theory of reactions at electrified interfaces. *Phys. Chem. Chem. Phys.* **2016**, *18*, 17799–17804.

(66) Lück, J.; Latz, A. Modeling of the electrochemical double layer and its impact on intercalation reactions. *Phys. Chem. Chem. Phys.* **2018**, *20*, 27804–27821.

Graphical TOC Entry